Computers and Electronics in Agriculture 104 (2014) 84–92

Contents lists available at ScienceDirect

Computers and Electronics in Agriculture

journal homepage: www.elsevier.com/locate/compag

Simulation of image acquisition in machine vision dedicated to seedling elongation to validate image processing root segmentation algorithms

Landry Benoit [a], David Rousseau [b,*], Étienne Belin [a], Didier Demilly [c], François Chapeau-Blondeau [a]

[a] Université d'Angers, Laboratoire Angevin de Recherche en Ingénierie des Systèmes (LARIS), 62 Avenue Notre Dame du Lac, 49000 Angers, France
[b] Université de Lyon, CREATIS, CNRS UMR 5220, INSERM U1044, Université Lyon 1, INSA-Lyon, 69621 Villeurbanne, France
[c] GEVES, Station Nationale d'Essais de Semences (SNES), Rue Georges Morel, 49071 Beaucouzé, France

ARTICLE INFO

Article history:
Received 19 October 2013
Received in revised form 5 March 2014
Accepted 4 April 2014

Keywords:
Machine vision
Numerical validation
Image processing
Simulation
Seedlings

ABSTRACT

This article proposes a methodology for the numerical validation of image processing algorithms dedicated to the segmentation of roots of plants with machine vision. A simulator of plant growth is coupled to a simulator of the image acquisition to generate images of simulated plants associated with a known synthetic ground truth. The simulator incorporates parameters of the plant and parameters of the experimental imaging system acquiring the images. This opens the possibility to assess the impact of these parameters on the performance of any segmentation algorithm on unlimited populations of virtual plants. Illustrations of this approach are given for the segmentation in 2D of seedlings with several classical algorithms and also with an algorithm of recent introduction. The presented results can be easily extended to 3D and are therefore also appropriate for other segmentation algorithms of roots with imaging modalities adapted for 3D root tracking like X-ray or MRI.

1. Introduction

Machine vision applied to plant science is a field of growing interest (see for instance Gwo et al., 2013; Chéné et al., 2012; Belin et al., 2013, for recent studies in this journal). This is linked to the recent need in plant science for automated contactless high throughput measurement methods required to investigate the phenotype of large populations of plants in relation to their genotype under given environmental conditions (Furbank and Tester, 2011). The diversity of plant species together with the different possible observations scales of observation (cell, seed, seedling, meristem, leaf, branching structure, fruit, entire plant, canopy) open the way for the design of a variety of imaging systems dedicated to plant phenotyping (Gupta and Ibakari, 2014). However, certain problems are common throughout plant science such as the study of the growth of the shoot and roots (see Spalding and Miller, 2013, for a recent review), or the recognition of species from their leaves (Du et al., 2007; Soares and Jacobs, 2013; Gwo et al., 2013). And plant models like *Arabidopsis thaliana* or *Medicago truncatula* serve as references for the whole community of plant scientists. This helps define both the scale of observation and constraints for the design of automated imaging systems based on machine vision. Efficient practices in terms of light, choice of optics and imaging technology are being progressively disseminated thanks to the recent development of a network of phenotyping centers at an international scale (Fiorani et al., 2012). Common geometries of imaging systems have been developed by separate research groups for similar problems. In the case of seedling growth, for instance, the imaging system in Subramanian et al. (2013), French et al. (2009) and Benoit et al. (2013) are similar in terms of geometry. On the other hand, a wide range of image processing algorithms (Wang et al., 2009; Kimura and Yamasaki, 2003; Subramanian et al., 2013; French et al., 2009; Benoit et al., 2013) have been proposed and are now referenced on the Web (Lobet et al., 2013), and the performance of these algorithms has not yet been compared. An important reason for the lack of comparison is that the validation of image processing algorithms in plant science requires comparison with ground truth. This ground truth can be manually established by experts. A drawback of this approach is the need to consider inter and intra experts variability when comparing numerical results. Another possible approach would be to build some physical phantoms to establish a synthetic ground truth. One can imagine rigid 3D structures made of wood or plastic that mimic the spatial architecture of plants. This would be possible for adult plants with solid stems but is less feasible for young seedlings. To enable the comparison of the various approaches in terms of image processing, a useful contribution is therefore the numerical simulation. *In silico* experimentation on

* Corresponding author.
E-mail address: david.rousseau@univ-lyon1.fr (D. Rousseau).
URL: http://lisabiblio.univ-angers.fr/PHENOTIC/telechargements (D. Rousseau).

http://dx.doi.org/10.1016/j.compag.2014.04.001
0168-1699/

simulated plants makes it possible to test with unlimited populations of plants the impact of physical parameters of the simulated acquisition system on the accuracy of the information extracted, or the expected performance of image processing algorithms for given tasks. To our knowledge, numerical simulation environments of plant growth together with image acquisition have only been so far developed at the scale of the entire plant for field imaging on assemblies of plants under the OpenAlea software (see Pradal et al., 2008, for an introduction). Here for the first time, we extend this approach to the monitoring of the growth of seedlings. The remainder of the paper is organized as follows. We start with the description of the imaging system dedicated to seedling elongation we intend to simulate. We then detail the simulator of seedling elongation and image acquisition. After, we demonstrate the interest of our simulator by testing a recently introduced algorithm to separate overlapping seedlings. Finally we conclude and discuss the potentiality of this simulation approach for other imaging modalities and other informational tasks in plant science imaging.

2. Image acquisition

The imaging system we use as a generic reference in this paper is composed of a gray level camera and a backlight constituted with green light. Seeds are placed in a Petri dish containing a transparent nutrient (agar gel). The Petri dish is placed between the camera and the backlight. Seeds are oriented so as to respect the vertical gravitropism of plants. The backlight mode is chosen to prevent specular reflection on the cover of the Petri dish without losing information on the external shape of the plants. The imaging system used here is dedicated to heterotrophic growth corresponding to the stage where seeds and seedlings develop in the soil. To mimic obscurity as in the soil, we use a green light, just for image capture. Green was chosen because it corresponds to a minimum of absorption by the different photochromes in plants (Smith, 2000). To limit the influence of light on the development of plants and on experimental conditions (apparition of drops of water inside the cover of the Petri dish, local heating that would encourage the development of fungi, etc.), the light was switched on only during image acquisition. This imaging system, depicted in Fig. 1, allows the acquisition of sequences of images similar to those shown in Fig. 2 which are useful to characterize the continuous development of each seedling from time zero (when the dry seed is placed on the agar gel) at an acquisition frequency determined by the user depending on the time scales being investigated. We tested this imaging system on different species including the model plant *Medicago truncatula*, rape, sugar beet, and wheat as shown in Fig. 3. In the sequel, we propose to simulate the image acquisition step of this imaging system so as to serve as a general framework for the validation of any image processing algorithm dedicated to the extraction of information from a sequence of images produced by such imaging systems.

3. Simulator

3.1. Description

Here we present the numerical validation method of algorithms for image processing of roots. This numerical method, described in Fig. 4 is composed of three stages:

- Stage 1: A seedling simulator establishes a ground truth.
- Stage 2: An acquired image simulator constitutes the images to be processed by the algorithm being tested.
- Stage 3: A comparison between the ground truth and the results produced by the algorithm being tested.

The principal of this numerical validation method can be applied to test any image processing algorithm. In this report, we use seedling segmentation as an illustration. The aim is therefore to objectively assess the performance of good and bad classifications of pixels between the background and the seedlings after a segmentation algorithm.

3.2. Seedling simulator

The seedling simulator is based on the L-system process described in Leitner et al. (2010). As illustrated in Fig. 5, the simulator in Leitner et al. (2010) enables the accelerated elaboration of root systems simulated in 3D without information on root width. We bring two upgrades on this algorithm. The first is the generation of spherical seeds at initial time. The second is the addition of an information on root width. The parameters used by this simulator are the size of the seeds, the width of the roots, the number of roots per seedling and the duration of the simulation. The seedling simulator in Leitner et al. (2010) generates root systems in 3D. The camera used in the imaging system in Fig. 1 does not access information on depth. We have therefore decided to build a plant simulator that generates a synthetic ground truth in two dimensions similar to the one shown in Fig. 6. This adaptation consists in projecting the synthetic ground truth in 3D onto a vertical plane. The synthetic ground truth produced by this seedling simulator is recorded as binary image with zero in seedlings and one in the background. The elongation rate of the root is a fixed parameter in Leitner et al. (2010). We did not modify it since at the scale of a Petri dish this produces sequences of simulated root systems with elongation rates similar to the one observed in real

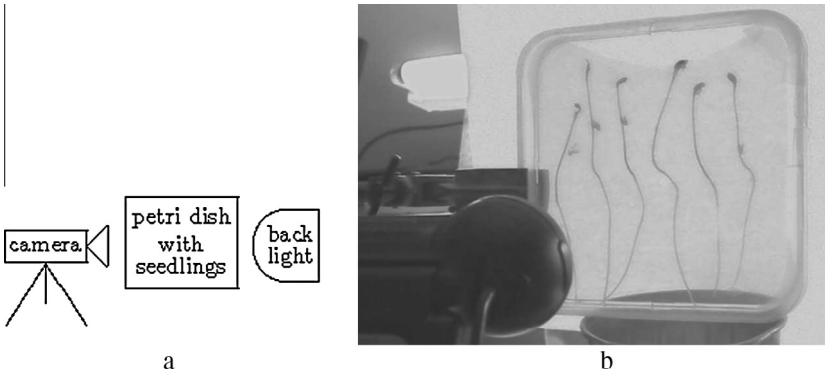

Fig. 1. The imaging system simulated in this report. Panel (a) schematic description and panel (b) lateral view of the setup. The camera is a Logitech C9600 webcam equipped with Zeiss optics and a CCD sensor with 1500 by 1200 pixels and a 8-bit resolution. The green light is produced by Luxeon LED. Most of the spectrum distribution of the LED is centered on 525 nm.

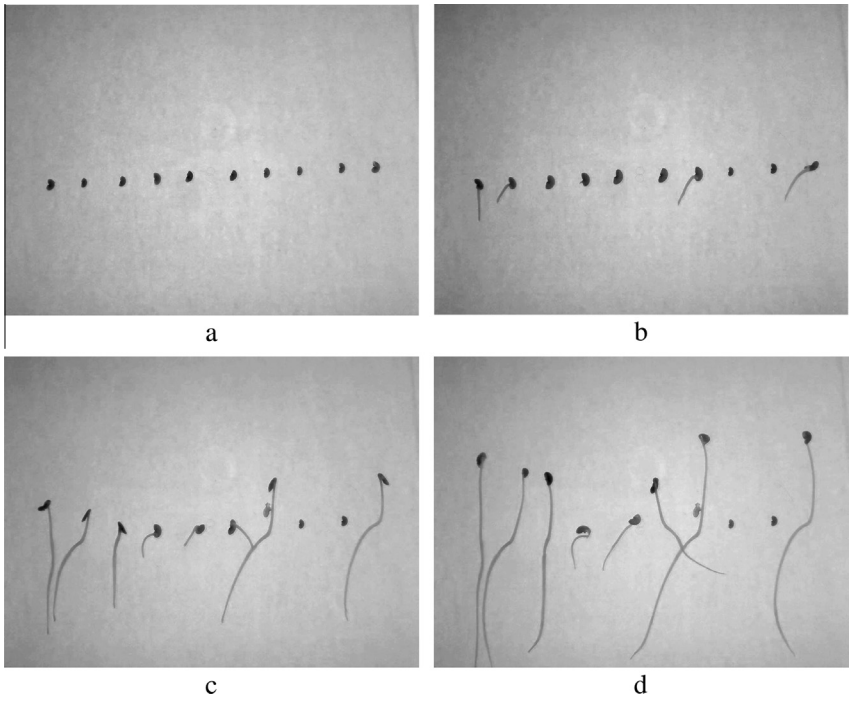

Fig. 2. Four gray level images of seedlings of *Medicago truncatula* during the elongation phase, from (a) to (d), acquired at 4 hourly intervals using the imaging system described in Fig. 1.

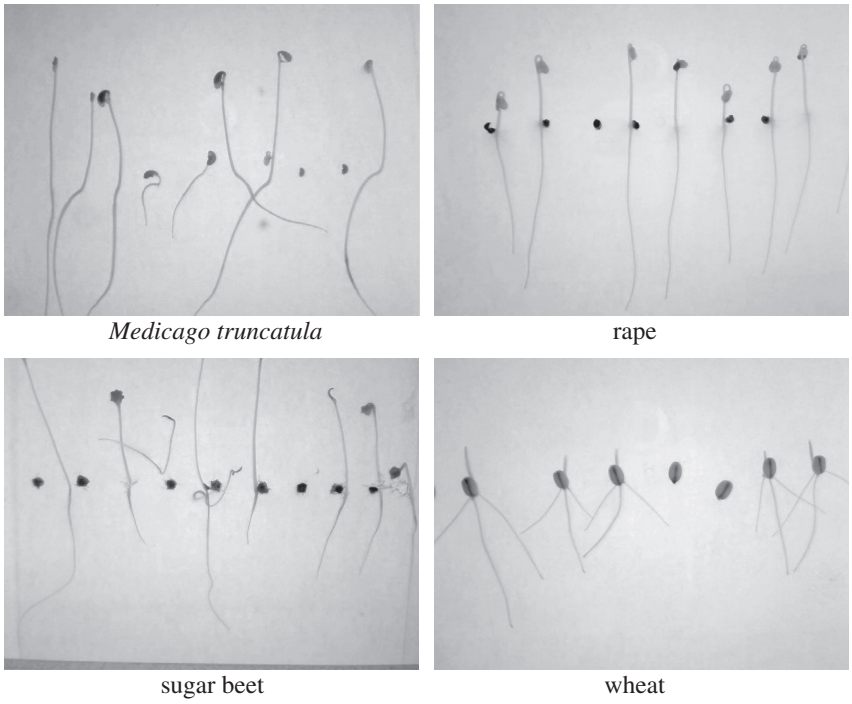

Fig. 3. Gray level images of seedlings from four different species acquired using the imaging system described in Fig. 1.

experimental conditions at temperature 20 Celsius with images of seedlings acquired at a time step of 1–4 images per hour.

3.3. Acquired image simulator

The acquired image simulator operates on the synthetic ground truth as depicted in Figs. 5 and 6, and constructs images of seedling that mimic actual images as they could be acquired from the imaging system shown in Fig. 1. Our modeling of the imaging system incorporates factors such as the spatial nonuniformity of backlight, light transmittance by the Petri dish and by the seedling, the imaging system characteristics, the effect of image compression.

We now explain how these simulated images were made. First we recorded images of a Petri dish only containing the agar gel. The diagonal plots in Fig. 7 show a spatial nonuniformity and the presence of random noise. To reproduce similar properties of the light,

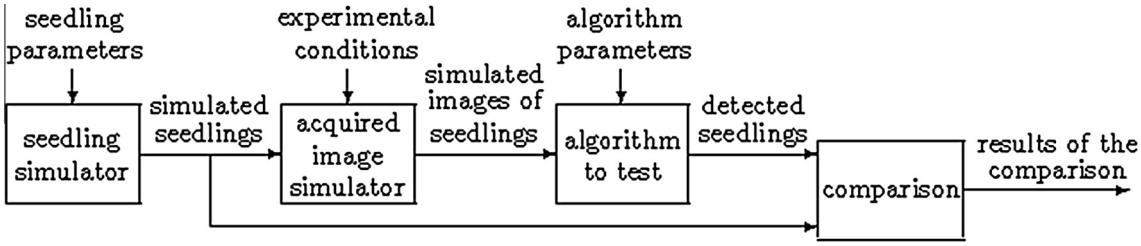

Fig. 4. Principle of the numerical method used to validate image processing algorithms of seedling images. Seedling parameters include the width of the seedling and their transmittance. Experimental conditions include spatial nonuniformity of the backlight, light transmittance by the agar gel, the characteristics of the imaging system and the effect of image compression.

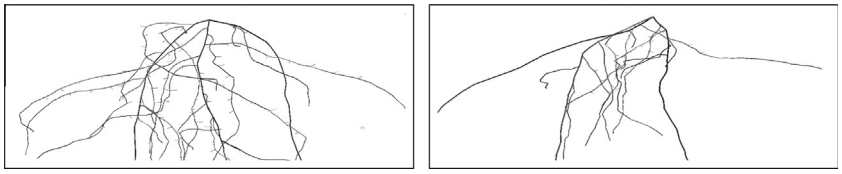

Fig. 5. Two simulated root systems using the generation algorithm described in Leitner et al. (2010).

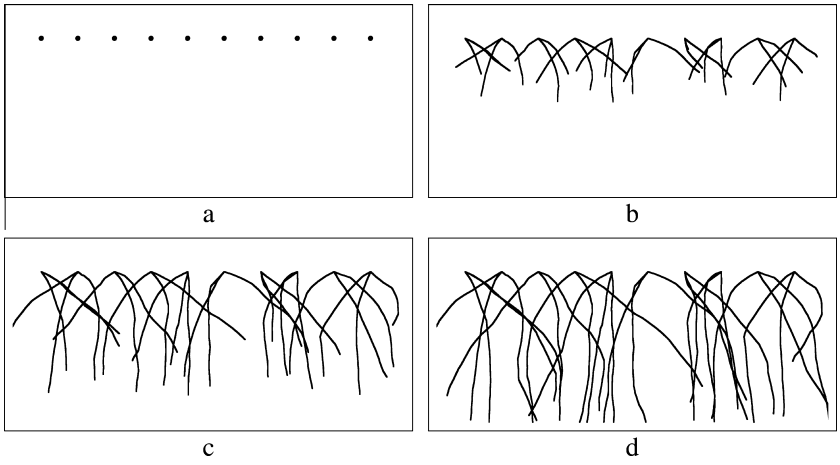

Fig. 6. Ten simulated seedlings from (a) to (d) in phase of elongation constituting a synthetic ground truth for testing seedling segmentation algorithms. Seed surface and root width are obtained from the analysis of real seedlings whose details are listed in Fig. 10.

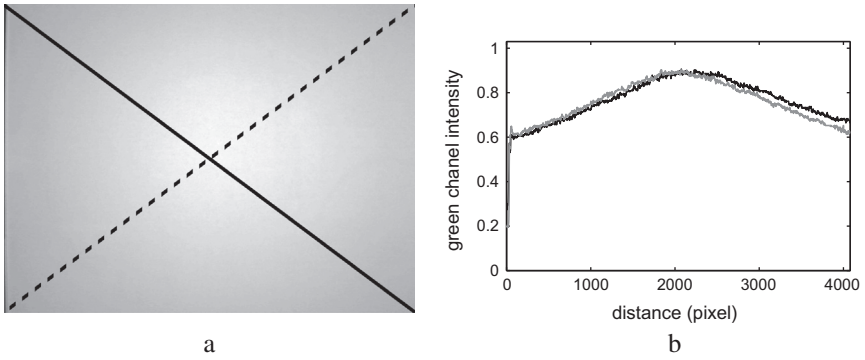

Fig. 7. Panel (a), image of a Petri dish with agar only acquired with the imaging system of Fig. 1. Panel (b) shows the evolution of pixel intensity along the diagonal in image (a) (— in black and -- in gray).

we call $I_{light}(x,y)$, with x,y spatial coordinates, the spatial intensity emitted from the backlight source. We model $I_{light}(x,y)$ as a two-dimensional Gaussian function with standard deviation σ

$$I_{light}(x,y) = I_0 \times \exp\left(-\frac{1}{2}\frac{(x-x_0)^2+(y-y_0)^2}{\sigma^2}\right), \quad (1)$$

where I_0 controls the overall level of light and x_0 and y_0 are the coordinates of the pixel at the center of $I_{light}(x,y)$. Eq. (1) therefore models the possibility of nonuniform light which can be reduced in our model with very large σ giving a truly uniformly lit plate. Our model makes it possible to test the impact of this parameter on the segmentation of the seedlings. This is what is experimented

with the imaging system in Fig. 1 because for mecatronic reasons (not to be detailed here) the backlight cannot be in contact with the agar plate. Eq. (1) is a common model for a bell-shaped illumination field, which is used in several areas of optics. It could be motivated by statistical arguments governing the random diffusion of individual photons. It also provides a simple and flexible model with a good fit to our measured data, and is accurate enough for the simulation of the imaging system we are considering here. However, this is not a critical point of the methodology, and other models could be used to simulate the illumination field of other imaging systems. Next, we model the transmittance of the agar in Petri dish with $I_{agar}(x,y)$. The noise due to agar gel has various origins. This includes nonuniform optical diffusion, due to nonhomogeneity of the thickness of agar gel or local aggregates of water droplets present inside the cover of the box, or again as observed in Subramanian et al. (2013) spurious artifacts due to air bubbles. Examples of all these sources of noise are illustrated in Fig. 8. For these reasons, it would be difficult to propose a simple theoretical model of I_{agar}. Instead, we propose an empirical model by recording a bank of images of real Petri dishes randomly including the described nonuniformities.

In optics, the action of a partially transparent medium on a parallel beam is modeled by multiplying the beam profile by the transparency of the optical medium. The transmittance of the Petri dish $I_{box}(x,y)$ can therefore be calculated as

$$I_{box}(x,y) = I_{agar}(x,y) \times I_{light}(x,y). \quad (2)$$

An example of an image simulated by Eq. (2) is given in Fig. 9 which appears to be in good agreement with the experimental images of the Petri dish in Fig. 7. Similarly to Eq. (2), the action of the transmittance T of the seedling can be simulated as

$$I_{seedling}(x,y) = T \times I_{box}(x,y) \quad (3)$$

in each pixel (x,y) where there is a seedling and

$$I_{seedling}(x,y) = I_{box}(x,y) \quad (4)$$

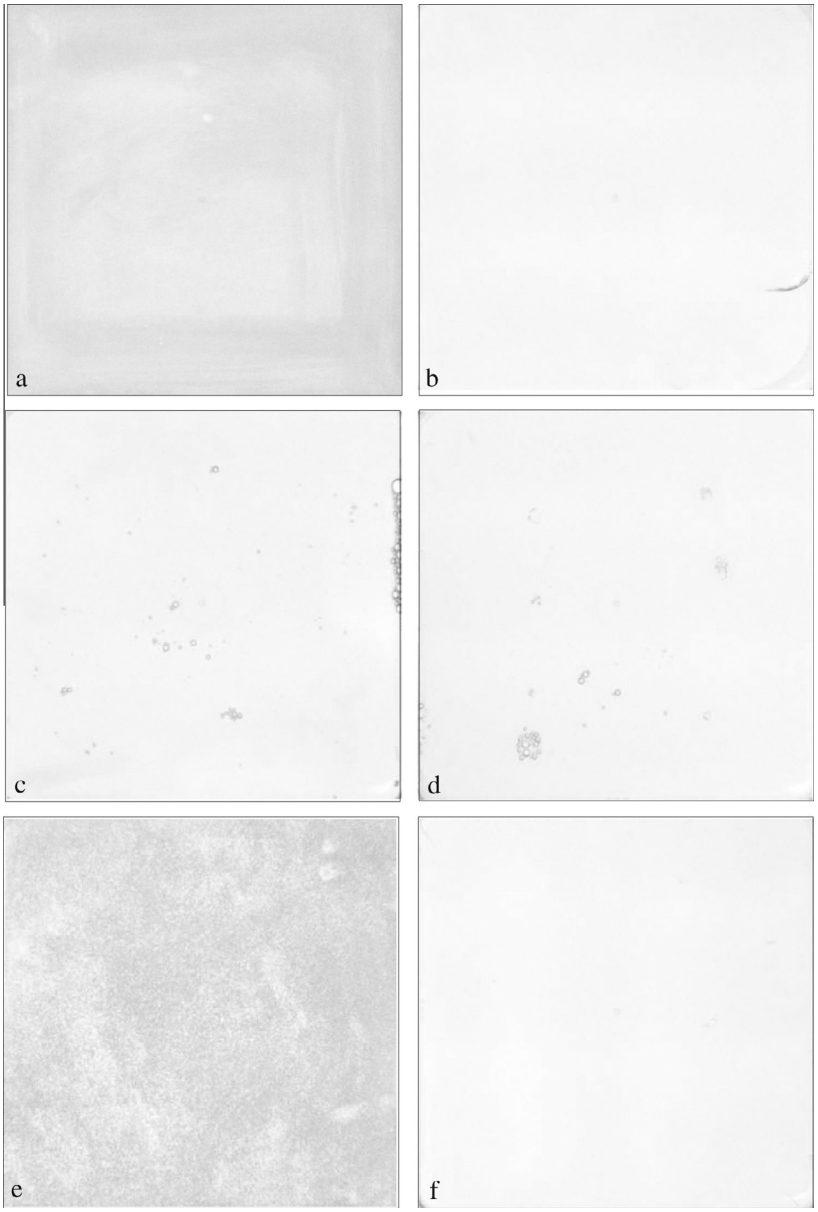

Fig. 8. Examples of the agar gel transmittance $I_{agar}(x,y)$ used in the acquired image simulator. (f) is free from artifacts while (a) shows nonuniform agar gel distribution, (b) includes an agar gel fissure, (c) and (d) contain air bubbles and (e) contains water droplets.

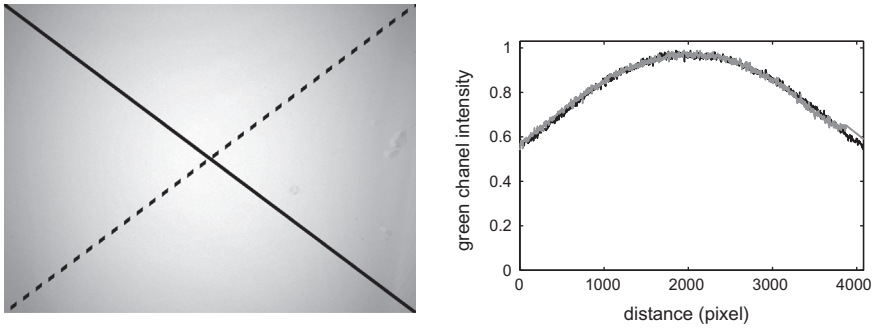

Fig. 9. Same as Fig. 7 but with simulated images from Eqs. (1) and (2).

in pixels located in the background and associated with a unit transmittance. The transmittance T of seedling is estimated as the average of a set of numerous observations. To this end, boxes with agar gel and seedlings are placed under uniform backlight. The estimation procedure of the transmittance T of the seedlings then consists in computing the ratio of average luminance transmitted in the area in which the seedling is located with the average luminance in the surrounding agar gel. The average transmittance estimated value for the four species presented in Fig. 3 are given in the table in Fig. 10. The combination of Eqs. (1)–(4) produces simulated images of seedlings like the ones displayed in Fig. 11.

A software version of our simulator is available online at http://lisabiblio.univ-angers.fr/PHENOTIC/telechargements. It runs under Matlab 7.5 and further versions with requirement of the "image processing" toolbox. We developed the user friendly interface shown in Fig. 12. In addition to the generation of simulated seedlings this software makes it possible to simulate image acquisition with ground truth loaded by the user that may come from manual or automated segmentation of real plants.

species	*Medicago Truncatula*	rape	sugar beet	wheat
transmittance T	0.87	0.95	0.91	0.96
seed surface (mm^2)	8.5	4.9	13.2	22.3
root width (mm)	1.7	0.9	1.3	0.7

Fig. 10. Three seedling parameters estimated from numerous images like the ones shown in Fig. 3.

4. Results

We are now ready to use the simulator presented in the previous section for the evaluation of a segmentation process on the seedling images. Segmentation performance, on a pixel by pixel count, is expressed as the rate of correct classifications and rate of false positives. H_0 is the hypothesis that a pixel belongs to the background and H_1 is the hypothesis that a pixel belongs to a seedling. Let us call D_0 the decision to classify a pixel as belonging to the background and D_1 the decision to classify a pixel as belonging to a seedling. The segmentation algorithm is evaluated by computing the probability of good detection defined as $P(D_1|H_1)$ and the probability of false positive defined as $P(D_1|H_0)$.

We tested three segmentation algorithms with our simulator:

- Global thresholding with the Otsu (1979) criterion applied on the entire image.
- Local thresholding with the Otsu criterion applied on a square of side twice the maximal width of a seedling.
- The local image processing algorithm recently described in Benoit et al. (2013) which was designed to segment and separate overlapping or crossing seedlings.

This comparison of the newly introduced algorithm with basic methods like global and local thresholding illustrates the interest

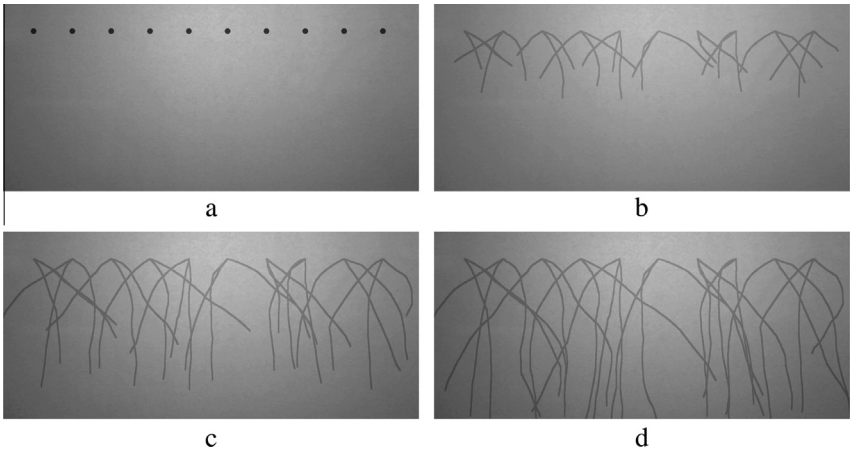

Fig. 11. Four simulated seedling gray images generated using the simulator of the acquired images. The simulator allows to generate images of seedlings in phase of elongation from seeds (a). The simulated Petri dish and the simulated seedlings of Fig. 6 have been used to construct this simulated seedling RGB images.

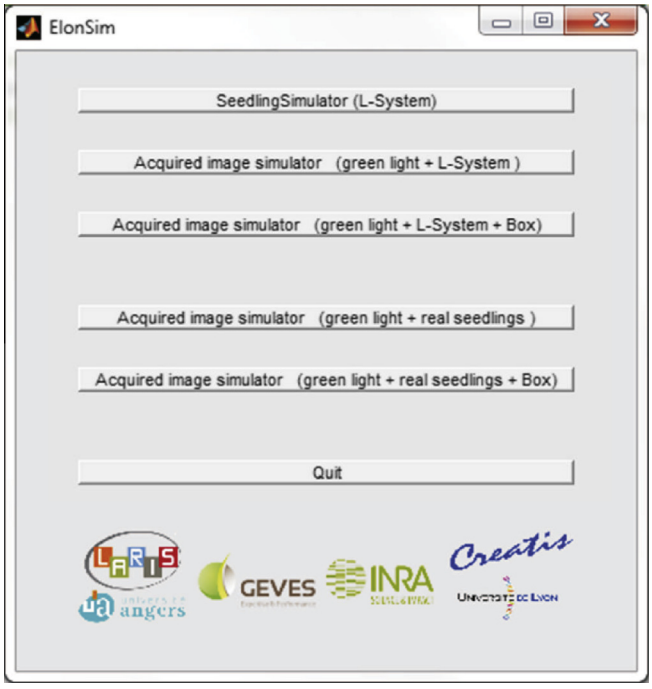

Fig. 12. User interface of our simulator which incorporates the seedling simulator and image acquisition simulator in the flow chart in Fig. 4. It is available online at http://lisabiblio.univ-angers.fr/PHENOTIC/telechargements.

of our numerical simulation. We first compare the performance of these three segmentation algorithms in different experimental conditions and various seedling parameters simulated with the simulator of the previous section. Fig. 13 shows the influence of the transmittance of seedling on the probability of good detection and on the probability false positive for a pixel in the image with the three algorithms listed above. As the seedling transmittance T increases from 0 to 1 in Fig. 13, the seedling becomes increasingly transparent and therefore increasingly difficult to distinguish from the background. Accordingly, the segmentation performance declines in Fig. 13 with increasing T although not in the same way for each of the three segmentation algorithms. Fig. 13 shows that the improvement of the algorithm in Benoit et al. (2013) is mainly its low probability of false positives compared with the global and local thresholding. In Fig. 14 we can assess the influence of the spatial nonhomogeneity of $I_{light}(x, y)$ on the performance of the three segmentation algorithms tested. Again the improvement of the algorithm in Benoit et al. (2013) is mainly its low probability of false positive compared with the global and local thresholding. We can also assess the influence of lossy compression on the performance of the segmentation algorithms and again see the superiority of the algorithm in Benoit et al. (2013) over the two other segmentation methods. JPEG compression is directly implemented on the simulated acquired images, using the standard approach available under Matlab 7.5.

To assess the predictive value of our simulator we compared its performance estimated from the images simulated by the simulator and estimated from images of real seedlings with ground truth realized manually by an expert. This was performed on the images of the real seedlings shown in Fig. 3. The results of the segmentation in terms of the probability of good detection and false positive are given in table of Fig. 16 for the three algorithms tested. The performance of segmentation is similar to the one predicted in Figs. 14–16 with a systematic difference (simulated-real) of 6%. The simulator thus provides useful quantitative characterizations to estimate the performances of seedling segmentation.

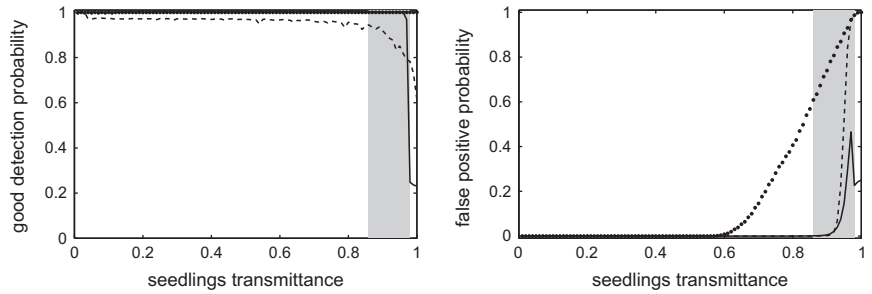

Fig. 13. Detection performance of the three compared segmentation algorithms as a function of seedling transmittance T. The dashed line represents global algorithm, the dots represents the local algorithm and the solid line represents the algorithm in Benoit et al. (2013). The gray zone corresponds to the range of transmittance of practical interest for the species depicted in Fig. 10.

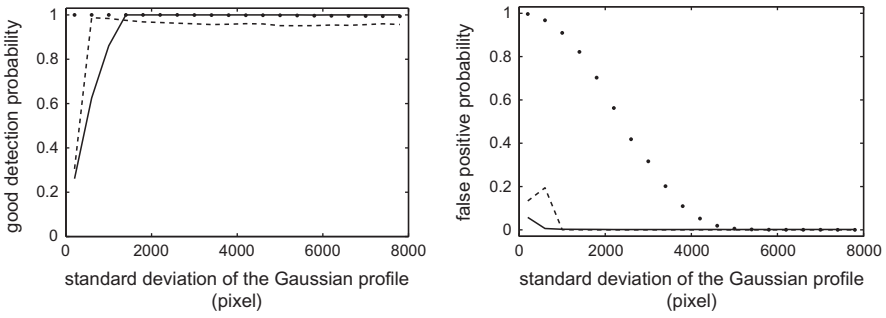

Fig. 14. Detection performance of the three compared segmentation algorithms as a function the standard deviation σ of the Gaussian distribution of $I_{light}(x, y)$. Dashed line is for the global algorithm, dots for the local algorithm and solid line is for the algorithm of Benoit et al. (2013). Seedling transmittance T is taken at $T = 0.87$ simulating seedlings of *Medicago truncatula*.

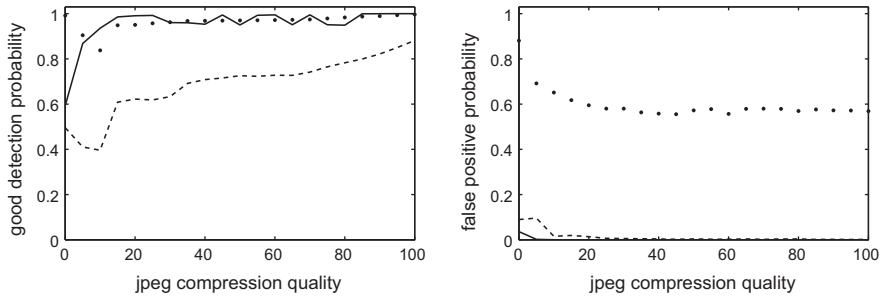

Fig. 15. Detection performance of the three compared segmentation algorithms as a function of the JPEG compression quality. Dashed line is for the global algorithm, dots for the local algorithm and solid line is for the algorithm of Benoit et al. (2013). Seedling transmittance T taken at $T = 0.87$ simulating seedlings of *Medicago truncatula*.

species	*Medicago truncatula*	rape	beet	wheat
good detection global segmentation	0.88	0.87	0.87	0.81
false positive global segmentation	0.34	0.41	0.53	0.64
good detection local segmentation	0.89	0.82	0.88	0.85
false positive local segmentation	0.08	0.23	0.18	0.25
good detection segmentation by (3)	0.95	0.92	0.92	0.87
false positive segmentation by (3)	0.05	0.10	0.09	0.24

Fig. 16. Results of the segmentation similar to the simulations of Figs. 13–15 but for the real seedlings shown in Fig. 3 by the three algorithms tested.

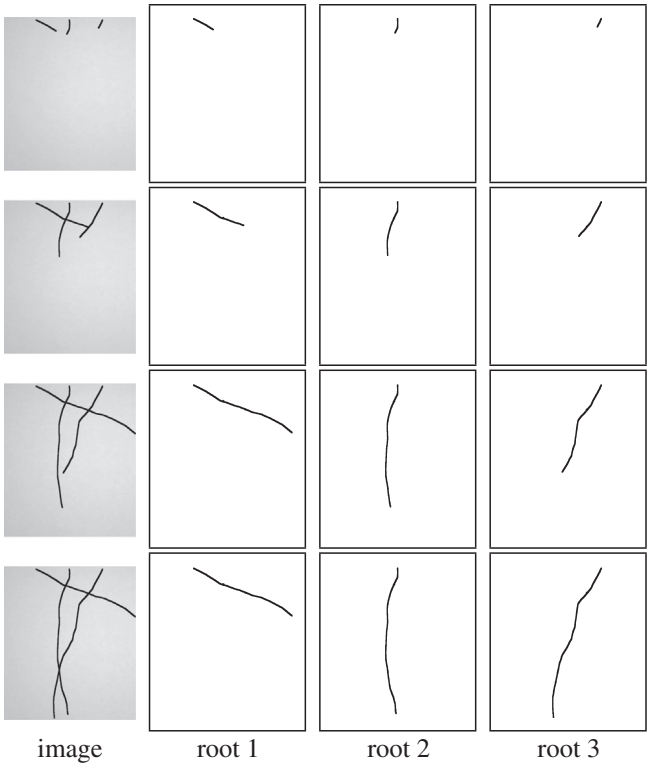

Fig. 17. Three simulated seedlings at different stages of elongation using the algorithm presented in Benoit et al. (2013). The first column gives the simulated images and the three other columns give the results from the segmentation and separation of the crossing seedlings.

We can now specifically test the capability of the algorithm in Benoit et al. (2013) to separate crossing seedlings. Fig. 17 illustrates the type of results obtained after correct separation of crossing seedlings. For a quantitative evaluation we display in Fig. 18 the probability of good crossing detection as a function of the transmittance T of seedlings.

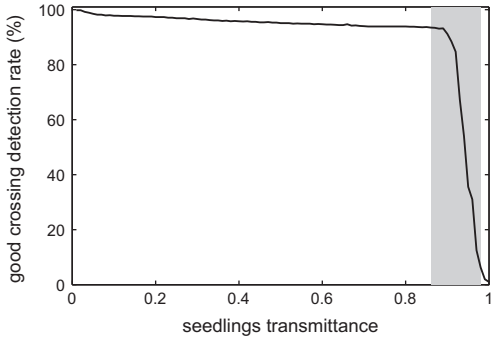

Fig. 18. Detection performance of the seedling crossing by the algorithm of Benoit et al. (2013) as a function of the transmittance T of the seedlings. The gray zone corresponds to the range of transmittance of practical interest for the species presented in Fig. 10.

5. Conclusion

We have presented a general methodology for the numerical validation of image processing algorithms applied to the segmentation of plant roots with an image acquisition system. We exploit the association of a simulator of plant growth coupled with an imaging system simulator. We illustrated this methodology using the problem of segmentation of seedling in elongation with a specific imaging system serving as a generic reference. The simulator incorporates parameters of the plant and parameters of the experimental conditions associated with the imaging system. The two major stages of the methodology described in this article are (i) a simulation model for the root system of the plant, on which operates (ii) a simulation stage of the image acquisition process. We described a basic setting for (i) and (ii), showing rather large flexibility and potentialities, and we developed an application to root segmentation. Further adaptation can be added to enrich this basic framework, and following the same line of the methodology to assess the impact of acquisition parameters on the performance of image processing algorithms on unlimited populations of virtual plants.

This work opens new perspectives for image processing of images of root systems. In this study we have used for illustration pixel by pixel evaluation of the segmentation. Higher level metrics like the total length or width of the seedlings could similarly be implemented to assess the quality of the segmentation of the seedlings. Also, the plant simulator used here works in 3D. It would therefore be possible to undertake the same numerical simulation for image processing of 3D images of roots. X-ray micro-computed tomography has recently been shown to be suitable for the segmentation of the architecture of root systems (Mairhofer et al., 2012). It would therefore be interesting to test the algorithm

described in Mairhofer et al. (2012) with the 3D plant simulator described in Leitner et al. (2010) following the simulation approach presented here in 2D with imaging in the visible spectrum. This would require a step of statistical modeling of the soil in X-ray. Soil are complex 3D with structures at multiple scales. In this context, fractal processes could be interesting models (Perfect, 1995; Caruso et al., 2011).

Acknowledgments

This work received support from the French Government supervised by the "Agence Nationale de la Recherche" in the framework of the program "Investissements d'Avenir" under reference ANR-11-BTBR-0007. Landry BENOIT gratefully acknowledges financial support from Angers Loire Métropole and GEVES-SNES for the preparation of his PhD.

References

Belin, E., Rousseau, D., Boureau, T., Caffier, V., 2013. Thermography versus chlorophyll fluorescence imaging for detection and quantification of apple scab. Comput. Electron. Agric. 90, 159–163.

Benoit, L., Rousseau, D., Belin, E., Demilly, D., Ducournau, S., Chapeau-Blondeau, F., Dürr, C., 2013. Locally oriented anisotropic image diffusion: application to phenotyping of seedlings; Special session GEODIFF, 8th International Joint Conference on Computer Vision, Imaging and Computer Graphics Theory and Applications (VISAPP 2013), Barcelona, Spain, 21-24 Feb. 2013.

Caruso, T., Barto, E.K., Siddiky, R.K., Smigelski, J., Rillig, M.C., 2011. Are power laws that estimate fractal dimension a good descriptor of soil structure and its link to soil biological properties? Soil Biol. Biochem. 43, 359–366.

Chéné, Y., Rousseau, D., Lucidarme, P., Bertheloot, J., Caffier, V., Belin, E., Chapeau-Blondeau, F., 2012. On the use of depth camera for 3D phenotyping of entire plants. Comput. Electron. Agric. 82, 122–127.

Du, J., Wang, X., Zhang, G., 2007. Leaf shape based plant species recognition. Appl. Math. Comput. 2, 883–893.

Fiorani, F., Rascher, U., Jahnke, S., 2012. Imaging plants dynamics in heterogenic environments. Curr. Opin. Biotechnol. 23, 227–235.

French, A., Ubeda-Tomás, S., Holman, T.J., Bennett, M.J., Pridmore, T., 2009. High-throughput quantification of root growth using a novel image-analysis tool. Plant Physiol. 150, 1784–1795.

Furbank, R.T., Tester, M., 2011. Phenomics-technologies to relieve the phenotyping bottleneck. Trends Plant Sci. 16, 635–644.

Gupta, S.D., Ibakari, Y., 2014. Plant Image Analysis: Fundamentals and Applications. CRC Press, Boca Raton.

Gwo, C., Wei, C., Li, Y., 2013. Rotary matching of edge features for leaf recognition. Comput. Electron. Agric. 91, 124–134.

Kimura, K., Yamasaki, S., 2003. Accurate root length and diameter measurement using NIH image: use of pythagorean distance for diameter estimation. Plant Soil 254, 305–315.

Leitner, D., Klepsch, S., Bodner, G., Schnepf, A., 2010. A dynamic root system growth model based on L-Systems. Plant Soil 332, 177–192.

Lobet, G., Draye, X., Périlleux, C., 2013. An online database for plant image analysis software tools. Plant Methods 9, 1–7.

Mairhofer, S., Zappal, S., Saoirse, R., Strurrock, T., Bennett, M., Mooney, S.J., Pridmore, T.P., 2012. RooTrak: automated recovery of three-dimensional plant root architecture in soil from X-ray microcomputed tomography using visual tracking. Plant Physiol. 158, 561–569.

Otsu, N., 1979. A threshold selection method from gray-level histograms. IEEE Trans. Syst. Man Cybernet. 9, 62–66.

Perfect, E., Kay, B.D., 1995. Application of fractals in soil and tillage research: a review. Soil Tillage Res. 36, 1–20.

Pradal, C., Dufour-Kowalski, S., Boudon, F., Fournier, C., Godin, C., 2008. OpenAlea: a visual programming and component-based software platform for plant modeling. Funct. Plant Biol. 35, 751–760.

Smith, H., 2000. Phytochromes and light signal perception by plants-an emerging synthesis. Nature 407, 585–591.

Soares, J.V., Jacobs, D.W., 2013. Efficient segmentation of leaves in semi-controlled conditions. Mach. Vis. Appl. 24, 1623–1643.

Spalding, E.P., Miller, N.D., 2013. Image analysis is driving a renaissance in growth measurement. Curr. Opin. Plant Biol. 16, 100–104.

Subramanian, R., Spalding, E.P., Frerrier, N.J., 2013. A high throughput robot system for machine vision based plant phenotype studies. Mach. Vis. Appl. 24, 619–636.

Wang, L., Assadi, A.H., Spalding, E.P., 2009. Tracing branched curvilinear structures with a novel adaptive local PCA algorithm. Plant Physiol. 53, 1632–1637.